



Published in final edited form as:

Contrast Media Mol Imaging. 2015 November ; 10(6): 481–486. doi:10.1002/cmml.1651.

Concentration-independent MRI of pH with a dendrimer-based pH-responsive nanoprobe

Mohammed P. I. Bhuiyan^a, Madhava P. Aryal^a, Branislava Janic^a, Kishor Karki^a, Nadimpalli R. S. Varma^a, James R. Ewing^a, Ali S. Arbab^b, and Meser M. Ali^{a,*}

^aHenry Ford Hospital, Detroit, MI, USA

^bDepartment of Biochemistry and Molecular Biology, Georgia Regents University, Augusta, GA, USA

Abstract

The measurement of extracellular pH (pH_e) has significant clinical value for pathological diagnoses and for monitoring the effects of pH-altering therapies. One of the major problems of measuring pH_e with a relaxation-based MRI contrast agent is that the longitudinal relaxivity depends on both pH and the concentration of the agent, requiring the use of a second pH-unresponsive agent to measure the concentration. Here we tested the feasibility of measuring pH with a relaxation-based dendritic MRI contrast agent in a concentration-independent manner at clinically relevant field strengths. The transverse and longitudinal relaxation times in solutions of the contrast agent (GdDOTA-4AmP)₄₄-G5, a G5-PAMAM dendrimer-based MRI contrast agent in water, were measured at 3 T and 7 T magnetic field strengths as a function of pH. At 3 T, longitudinal relaxivity (r_1) increased from 7.91 to 9.65 $\text{mM}^{-1} \text{s}^{-1}$ (on a per Gd^{3+} basis) on changing pH from 8.84 to 6.35. At 7 T, r_1 relaxivity showed pH response, albeit at lower mean values; transverse relaxivity (r_2) remained independent of pH and magnetic field strengths. The longitudinal relaxivity of (GdDOTA-4AmP)₄₄-G5 exhibited a strong and reversible pH dependence. The ratio of relaxation rates R_2/R_1 also showed a linear relationship in a pH-responsive manner, and this pH response was independent of the absolute concentration of (GdDOTA-4AmP)₄₄-G5 agent. Importantly, the nanoprobe (GdDOTA-4AmP)₄₄-G5 shows pH response in the range commonly found in the microenvironment of solid tumors.

Keywords

responsive agent; noninvasive pH measurement; magnetic resonance imaging; dendritic agent

1. INTRODUCTION

The extracellular tumor microenvironment is characterized by an acidic pH (denoted pH_e to identify it as the extracellular pH), and an intracellular pH_i (1–5) that is neutral to alkaline.

A similar transcellular pH gradient is not observed in normal tissues. Contributing factors to

*Correspondence to: M. M. Ali, Henry Ford Hospital, Detroit, MI, USA. mali8@hfhs.org.

SUPPORTING INFORMATION

Additional supporting information may be found in the online version at the publisher's web site.

an acidic tumor pH_e are increased glycolysis, even in the presence of sufficient oxygen (the Warburg effect) (6). Hydrolysis of ATP is also a significant contributor to acidosis in tumors during acute hypoxia. The tumor microenvironment is intrinsically acidic, mainly due to accumulation of lactic acid as a result of increased aerobic and anaerobic glycolysis by tumor cells (7,8). Poor tissue perfusion and reduced buffering capacity in the extracellular tumor microenvironment aggravates the decrease in tumor pH_e (9,10). A lower pH_e in tumors has been correlated with increased gene mutation (11) and gene rearrangement rates (12,13), and altered gene expressions (14–21) that can lead to spontaneous transformation of non-metastatic tumors into metastatic tumors (22–26). A lower tumor pH_e can cause ion trapping and provide resistance to chemotherapies that act as weak bases (27–30), such as doxorubicin (31). In some cases, the lower tumor pH_e can enhance the efficacy of chemotherapies that act as weak acids (32–35). Thus, a method to estimate tissue pH that could both point to potentially resistant cases, and guide supplementary therapeutic strategies, might significantly improve clinical outcomes.

Previous work has shown that magnetic resonance imaging (MRI) can map pH_e throughout a tumor volume at high spatial resolution with good detection sensitivity in clinically reasonable time frames (36–38). However, the change in T_1 relaxation caused by a pH-responsive MRI contrast agent can also depend on the concentration of the agent. The tissue concentration of a pH-responsive agent can be estimated by using a second pH-unresponsive agent as a surrogate (36). However, this serial injection substantially prolongs the time of the study, a major disadvantage for clinical translation. Although a pH-unresponsive T_2^* relaxation contrast agent can be co-injected with a pH-responsive T_1 relaxation contrast agent, and the different T_2^* and T_1 effects can then be used to selectively detect each agent within the same tumor tissue, the strong correlations between T_1 relaxation and T_2^* relaxation create difficulties in quantifying each agent in the same tissue, making this approach extremely challenging (39). In brief, a concentration-independent technique for estimating tissue pH would significantly improve efforts to estimate pH_e by changes in T_1 relaxation rates.

To quantify the agent's concentration, the positron emission tomography (PET) isotope F-18 has been incorporated with a pH-responsive relaxation agent (GdDOTA-4AmP⁵⁻) to measure pH *in vitro* (40). PET was used to quantify the concentration of relaxation-based pH-responsive MRI probe (GdDOTA-4AmP⁵⁻). This approach required a multimodal MR-PET device, and reduced spatial resolution to that of the PET scanner. The ¹⁹F/¹H ratiometric method has also been used to measure pH (41). ¹⁹FMRS also suffers from coarse resolution and lack of clinically available MRI coils.

Recently, small molecule CEST and PARACEST contrast agents have been used to estimate *in vivo* pH by taking the ratio of the CEST effect from two different chemical shifts originating from the same molecule. Although these MRI CEST methods appear promising, they suffer from the low detection sensitivity of CEST agents in an *in vivo* application (42,43).

A concentration-independent method for the (GdDOTA)₃₃-poly-L-ornithine macromolecular MRI contrast agent has been proposed (44). This method used the ratio of

R_1 and R_2 relaxation rates, which is independent of concentration, but sensitive to pH for a macromolecular system. However, (GdDOTA)₃₃-poly-L-ornithine is sensitive only to a pH greater than 7, and shows limited dynamic range and sensitivity in the pH range from pH 6.5 to 8, the range most relevant *in vivo* to tumor physiology.

A macromolecule is needed that is pH sensitive in the range 6.5–8, and with an R_2/R_1 ratio that has a linear relationship to pH_e , independent of Gd^{3+} concentration. Previously, we succeeded in synthesizing a nanoscale, pH-responsive MRI contrast agent (Fig. 1) (45). Conjugation of the small molecule pH-responsive agent GdDOTA-4AmP⁵⁻ to the surface amines of a Generation 5 (G5) PAMAM dendrimer improved T_1 relaxivity with pH significantly at 0.5 T, 25 °C. Importantly, the nanoprobe (GdDOTA-4AmP⁵⁻)₉₆-G5 showed pH response in the physiological range of 6.0–8.0.

In this report, we present (GdDOTA-4AmP⁵⁻)₄₄-G5, a modified version of the previous G5 PAMAM dendrimer. This new compound has a reduced negative surface charge, thus higher biocompatibility, and a higher potential for drug conjugation than previous compounds, thus improving its theranostic potential. For a relevant *in vivo* application in preclinical models, it is necessary to investigate pH response at the higher field strengths, where animals are usually scanned. In this report, we study the longitudinal and the transverse relaxation properties of this (GdDOTA-4AmP⁵⁻)₄₄-G5 conjugate at 3 T and 7 T.

2. RESULTS AND DISCUSSION

A pH-responsive GdDOTA-4AmP⁵⁻ analogue was conjugated to the surface amines of a G5-PAMAM dendrimer via an isothiocyanatobenzyl group using methods previously reported (45). In that report, we conjugated 96 (GdDOTA-4AmP⁵⁻) chelates on the surface of a G5 PAMAM dendrimer, thus leading to a highly negative charged paramagnetic nanoparticle. The present study presents a modification of that synthetic method. A MALDI-TOF analysis showed an average of 44 (GdDOTA-4AmP⁵⁻) chelates in the nanostructure (Supplementary Fig. 1). The GdDOTA-4AmP⁵⁻ complex has four appended phosphonate groups, with variable pK_a values ranging from 6.0 to 8.0 (37,38). When the protons of the phosphonate group dissociate at their respective pK_a values, the chelate gains a negative charge up to a value of -5 , while it has either neutral or positive charge below these pK_a values (38). That is to say, a phosphonate-based MRI contrast agent has charge reversal properties.

We observed the pH response of this dendrimeric agent. The absolute detection sensitivity of the nanoscale MRI contrast agent showed a robust improvement relative to the monomeric agent (38) at 3 T. The average r_1 relaxivity of Gd₄₄-G5 conjugate per dendrimer was a sizable $348 \text{ mM}^{-1} \text{ s}^{-1}$ at pH 8.84, rising to $425 \text{ mM}^{-1} \text{ s}^{-1}$ at pH 6.35 (Fig. 2). At 7 T, the r_1 relaxivity of Gd₄₄-G5 decreased significantly for all pH values (Fig. 2); this is the typical behavior of the r_1 relaxivity of large molecules with increasing field strength (46). Nevertheless, compared with the monomer, the r_1 relaxivity of Gd₄₄-G5 still showed pH response at high field strength (38), and the detection sensitivity of the Gd₄₄-G5 dendrimeric conjugate improved by a factor of two at 3 T for all pH values. Thus, compared with a monomeric agent, a lower injection dose of Gd₄₄-G5 dendrimeric conjugate will be required

for *in vivo* applications. GdDOTA-4AmP has been tested in biological fluid (40). In the presence of Ca(II), Cu(II), and Zn(II) ions (38) there was no change in pH-dependent relaxivity profiles. In addition, the agent has been applied in tissues (47), perfused tissues or organs or *in vivo* (48), with the result that GdDOTA-4AmP did not interact in biological fluids or in the presence of ions.

The r_1 relaxivity of Gd₄₄-G5 showed pH response at both field strengths, while r_2 relaxivity remained independent of pH and magnetic field strength (Fig. 2). The R_2 values at 3 T were not significantly larger than those at 7 T, and the r_2 profiles (slopes) at the two field strengths were essentially the same. As for r_1 versus pH, the slopes of r_1 versus pH at 3 T and 7 T are essentially the same.

The pH-responsive r_1 relaxation properties of GdDOTA-4AmP⁵⁻ were first reported by the Sherry group (38). This agent responds to pH by changes in proton exchange (variable τ_M). The compound has four appended phosphonate groups that have pK_a values in the range 6.0–8 (37,38), and as these phosphonate groups become protonated below $pH \approx 8$ the monoprotonated phosphonate groups hydrogen bond (38) with the single Gd³⁺-bound water molecule and catalytically exchange the highly relaxed bound water protons with protons of bulk water (45). To understand the origin of pH-sensitive r_1 relaxation properties of dendrimer-based GdDOTA-4AmP conjugate, nuclear magnetic resonance dispersion (NMRD) profiles were studied in our previous report (45). NMRD profiles revealed that multiple factors are involved in pH sensing r_1 relaxation properties of this agent. The pH response was the result of a complex interplay between the rate of proton exchange between the bulk solvent and water molecules in the inner and second hydration spheres (45). In contrast to r_1 relaxation properties of (GdDOTA-4AmP)₄₄-G5 agent, the r_2 relaxation properties remain essentially independent of pH, as shown in Fig. 2. We did not observe a significant difference in r_2 relaxation properties at either 3 T or 7 T, which is consistent with the reported r_2 relaxation properties of manganese complexes (46).

Silvio Aime and co-workers (44) reported a novel method based on a ratiometric approach that consists of measuring the ratio between the transverse and the longitudinal paramagnetic contribution to the water proton relaxation rate, i.e. R_{2p}/R_{1p} of a macromolecule at magnetic field strength higher than 0.2 T. The ratio, R_{2p}/R_{1p} , of water protons becomes independent of Gd³⁺ concentration for a motionally restricted agent, (GdDOTA)33-poly-L-ornithine ($\tau_R > 1$ ns), but remains dependent on τ_M , τ_R and other magnetic parameters that normally affect relaxation in these complexes. We applied this R_2/R_1 ratiometric approach to our dendrimer-based (Gd-DOTA-4AmP)₄₄-G5 system.

In order to examine our hypothesis that (Gd-DOTA-4AmP)₄₄-G5 measures pH as a single agent without knowledge of the agent's concentration, we measured the ratio of R_2 and R_1 relaxation rates of (Gd-DOTA-4AmP)₄₄-G5 at four different Gd³⁺ concentrations with three different pH values at 7 T (Fig. 3). For three concentrations, the mean values of R_2/R_1 are 8.24 ± 0.05 , 8.98 ± 0.12 , and 10.02 ± 0.05 for pH values of 6.96, 7.40, and 8.84, respectively. The slopes of the three plots of R_2/R_1 are 0.03 ± 0.06 , -0.05 ± 0.15 , and 0.08 ± 0.03 , respectively. The slope of R_2/R_1 is significantly nonzero at the highest pH ($pH = 8.84$). However, this pH is outside the range of physiological value in tumors, and the variation

across even the range of concentrations reported is only about 6%. Thus, we conclude that the R_2/R_1 ratio is essentially independent of concentration for each pH value.

In order to further examine the ratiometric approach, R_1 , R_2 , and R_2/R_1 (Fig. 4(A)–(C), respectively) maps for six different pH values at 7 T for a given Gd^{3+} concentration were generated. The ratio of R_2/R_1 maps of the phantoms containing solutions of different pH with added (Gd-DOTA-4AmP)₄₄-G5 were plotted versus pH for both 7 T and 3 T data, along with the 95% confidence intervals for their regressions. Figure 5 demonstrates that the ratio R_2/R_1 was pH responsive at both field strengths. The two slopes are 1.18 ± 0.11 and 0.330 ± 0.091 for 7 T and 3 T curves, respectively, and the y-intercepts are -0.36 ± 0.81 and -0.94 ± 0.69 , again for 7 T and 3 T. Neither of the intercepts is significantly different from zero. The ratio R_2/R_1 increased from 3.23 to 4.05 and from 7.04 to 10 pH units, at 3 T and 7 T respectively, on changing the solution pH from 6.35 to 8.84. It is apparent that the accuracy of the 3 T methods is lower than that of the 7 T methods. We do not believe this to be intrinsic to the field strengths, but it is clear that a careful calibration of both T_1 and T_2 methods, particularly with regard to flip angles, is required for accuracy in reading out the ratio of R_2/R_1 as an estimate of pH.

3. CONCLUSION

In this study, a novel pH-responsive dendrimer-based MRI contrast agent (Gd-DOTA-4AmP)₄₄-G5 was evaluated as a potential pH imaging agent at 3 T and 7 T magnetic field strengths. In general, the compound exhibited good dynamic range in a concentration-independent parameter (R_2/R_1) across physiologically significant pH values. The improvement of R_2/R_1 values for this nanostructure, 1.19 per pH unit, is almost double that of the previously reported R_2/R_1 values for a ratiometric pH-responsive probe (44). These findings support the expectation that the agent can be used to estimate tumor pH *in vivo* by means of estimates of changes in the R_2/R_1 ratio after administration of (Gd-DOTA-4AmP)₄₄-G5. The ratiometric approach to measure pH does not require knowledge of the concentration of the agent. (Gd-DOTA-4AmP)₄₄-G5 with T_1 and T_2 effects constitutes a single MRI contrast agent that can accurately measure pH_e in a concentration-independent manner at clinically relevant magnetic field strengths.

4. EXPERIMENT

4.1. Synthesis

We have synthesized a modified version of the pH-responsive MRI nanoprobe GdDOTA-4AmP-G5 by following our published synthetic method (45). The final conjugate was purified by diafiltration using a Centricon C-30 cell with a 30 kDa molecular weight cut-off, after which the solvents were removed by lyophilization to afford a colorless solid (0.19 g). The MW of the p-SCN-DOTA-4AmPE conjugated G5 dendrimer was estimated at 79 082 g/mole by MALDI-TOF analysis (Supplementary Fig. 1). This corresponds to a G5-dendrimer with an average of 44 chelated Gd^{3+} ions per dendrimer. The number of chelates per dendrimer unit was also obtained using the same method as in our previous report (45). To examine our hypothesis, we prepared phantoms of [(GdDOTA-4AmP)₄₄-G5] at four or

five different concentrations with six different pH values. Gd^{3+} concentration was determined by ICP analyses.

4.2. MRI Methods

MRI experiments were performed on a 3.0 T clinical system (Signa Excite, GE Health) using 50 mm diameter \times 108 mm RF rung length (Litzcage small animal imaging system, Doty Scientific, Columbia, SC). Multi-echo T_2 -weighted (T_2W) images and T_1 -weighted (T_1W) images using three dimensional spoiled gradient echo (3D SPGR) were acquired. T_2W images were obtained using standard two-dimensional Fourier transformation (2DFT) multi-slice (15 slices) multi-echo MRI sequences with an echo time (TE) of 11, 22, 33, and 44 ms and a repetition time (TR) of 2000 ms, field of view (FOV) of 30 mm, 1mmslice thickness, and matrix size of 128×128 . The T_1W images were acquired using 3D SPGR with the following parameters: $TR = 9.46ms$, $TE = 1.732ms$, 128×128 matrix size, FOV = $40 \times 40 \times 40$ mm³, effective slice thickness = 1 mm, and flip angles = 2°, 4°, 8°, 12°, 15°, 20°, 25°, 30°, 35°. The R_2 ($1/T_2$) maps were calculated from the acquired T_2W images at eight different TE values using a log-linear least square fit on a pixel-by-pixel basis by following the reported method (49). The T_1 maps were calculated from the acquired T_1W images at nine different flip angles using a linear least square fit (on a pixel-by-pixel basis) (50). The calculated value of T_1 was inverted to generate the R_1 map.

For measurements of T_1 and T_2 relaxation times on a 7 T Varian system, axial spin echo (SE) sequences were obtained with multiple TR (50, 100, 200, 300, 500, 750, 1000, 1500, 2000, 3000, and 5500 ms) and TE (8.4, 16.8, 25.2, and 33.6 ms) values. All sequences were acquired with FOV = 24 mm₂, matrix size = 128×64 , one slice, thickness = 1 mm, and $N_{EX} = 1$. MR images were transferred to an off-line server and reconstructed using home-written software. T_1 and T_2 maps of the samples were calculated by fitting the appropriate relaxation equation to the image data, assuming monoexponential signal decay (for both T_1 and T_2) on a pixel-by-pixel basis. For T_1 maps, all echoes were summed for each TR and then fitted using the equation $M_z(t) = M_0[1 - \exp(-TR/T_1)]$. T_2 maps were generated by summing data across all TR values, and then fitting the summed values using the equation $M_{xy}(t) = M_0[\exp(-TE/T_2)]$. The longitudinal and transverse relaxation times of the Gd_{44} -G5 in solution were then measured in ROIs selected in the calculated sample maps.

Supplementary Material

Refer to Web version on PubMed Central for supplementary material.

Acknowledgements

The authors acknowledge research support from the National Institutes of Health (NIH) grants K25CA129173 (to MMA) and 1R01CA160216 (to ASA). We thank Professor Mark D. Pagel for helpful discussion.

REFERENCES

1. Delli Castelli D, Ferrauto G, Cutrin JC, Terreno E, Aime S. In vivo maps of extracellular pH in murine melanoma by CEST-MRI. *Magn Reson Med*. 2014; 71(1):326–332. [PubMed: 23529973]

2. Engin K, Leeper DB, Cater, Thistlethwaite AJ, Tupchong L, McFarlane JD. Extracellular pH distribution in human tumours. *Int J Hypertherm.* 1995; 11(2):211–216.
3. Garcia-Martin ML, Herigault G, Remy C, Farion R, Ballesteros P, Coles JA, Cerdan S, Ziegler A. Mapping extracellular pH in rat brain gliomas *in vivo* by ^1H magnetic resonance spectroscopic imaging: comparison with maps of metabolites. *Cancer Res.* 2001; 61(17):6524–6531. [PubMed: 11522650]
4. Gillies RJ, Liu Z, Bhujwala Z. ^3P -MRS measurements of extracellular pH of tumors using 3-aminopropylphosphonate. *Am J Physiol.* 1994; 267(1 Pt 1):C195–C203. [PubMed: 8048479]
5. van Sluis R, Bhujwala ZM, Raghunand N, Ballesteros P, Alvarez J, Cerdan S, Galons JP, Gillies RJ. *In vivo* imaging of extracellular pH using ^1H MRSI. *Magn Reson Med.* 1999; 41(4):743–750. [PubMed: 10332850]
6. Warburg O. On the origin of cancer cells. *Science.* 1956; 123(3191):309–314. [PubMed: 13298683]
7. Gatenby RA, Gillies RJ. Glycolysis in cancer: a potential target for therapy. *Int J Biochem Cell Biol.* 2007; 39(7/8):1358–1366. [PubMed: 17499003]
8. Gatenby RA, Gillies RJ. Integrated imaging of cancer metabolism. *Academic Radiol.* 2011; 18(8):929–931.
9. Schwickert G, Walenta S, Sundfor K, Rofstad EK, Mueller-Klieser W. Correlation of high lactate levels in human cervical cancer with incidence of metastasis. *Cancer Res.* 1995; 55(21):4757–4759. [PubMed: 7585499]
10. Jain RK. Determinants of tumor blood flow: a review. *Cancer Res.* 1988; 48(10):2641–2658. [PubMed: 3282647]
11. Bhujwala ZM, Aboagye EO, Gillies RJ, Chacko VP, Mendola CE, Backer JM. Nm23-transfected MDA-MB-435 human breast carcinoma cells form tumors with altered phospholipid metabolism and pH: a ^3P nuclear magnetic resonance study *in vivo* and *in vitro*. *Magn Reson Med.* 1999; 41(5):897–903. [PubMed: 10332871]
12. Stein I, Neeman M, Shweiki D, Itin A, Keshet E. Stabilization of vascular endothelial growth factor mRNA by hypoxia and hypoglycemia and coregulation with other ischemia-induced genes. *Mol Cell Biol.* 1995; 15(10):5363–5368. [PubMed: 7565686]
13. Cuvier C, Jang A, Hill RP. Exposure to hypoxia, glucose starvation and acidosis: effect on invasive capacity of murine tumor cells and correlation with cathepsin (L + B) secretion. *Clin Exp Metastasis.* 1997; 15(1):19–25. [PubMed: 9009102]
14. Scott PA, Gleadle JM, Bicknell R, Harris AL. Role of the hypoxia sensing system, acidity and reproductive hormones in the variability of vascular endothelial growth factor induction in human breast carcinoma cell lines. *Int J Cancer.* 1998; 75(5):706–712. [PubMed: 9495238]
15. Curthoys NP, Tang A, Gstraunthaler G. pH regulation of renal gene expression. *Novartis Found Symp.* 2001; 240:100–111. discussion 111–104. [PubMed: 11727924]
16. Fukumura D, Xu L, Chen Y, Gohongi T, Seed B, Jain RK. Hypoxia and acidosis independently up-regulate vascular endothelial growth factor transcription in brain tumors *in vivo*. *Cancer Res.* 2001; 61(16):6020–6024. [PubMed: 11507045]
17. Roboz GJ, Giles FJ, List AF, Cortes JE, Carlin R, Kowalski M, Bilic S, Masson E, Rosamilia M, Schuster MW, Laurent D, Feldman EJ. Phase 1 study of PTK787/ZK 222584, a small molecule tyrosine kinase receptor inhibitor, for the treatment of acute myeloid leukemia and myelodysplastic syndrome. *Leukemia.* 2006; 20(6):952–957. [PubMed: 16617323]
18. Turner GA. Increased release of tumour cells by collagenase at acid pH: a possible mechanism for metastasis. *Experientia.* 1979; 35(12):1657–1658. [PubMed: 42555]
19. Schlappack OK, Zimmermann A, Hill RP. Glucose starvation and acidosis: effect on experimental metastatic potential, DNA content and MTX resistance of murine tumour cells. *Br J Cancer.* 1991; 64(4):663–670. [PubMed: 1911214]
20. Bennett DC, Holmes A, Devlin L, Hart IR. Experimental metastasis and differentiation of murine melanoma cells: actions and interactions of factors affecting different intracellular signalling pathways. *Clin Exp Metastasis.* 1994; 12(6):385–397. [PubMed: 7923991]
21. Martinez-Zaguilan R, Martinez GM, Gomez A, Hendrix MJ, Gillies RJ. Distinct regulation of pH^{in} and $[\text{Ca}^{2+}]^{\text{in}}$ in human melanoma cells with different metastatic potential. *J Cell Physiol.* 1998; 176(1):196–205. [PubMed: 9618159]

22. Reshkin SJ, Bellizzi A, Albarani V, Guerra L, Tommasino M, Paradiso A, Casavola V. Phosphoinositide 3-kinase is involved in the tumor-specific activation of human breast cancer cell Na^+/H^+ exchange, motility, and invasion induced by serum deprivation. *J Biol Chem.* 2000; 275(8):5361–5369. [PubMed: 10681510]
23. Mahoney BP, Raghunand N, Baggett B, Gillies RJ. Tumor acidity, ion trapping and chemotherapeutics. I. Acid pH affects the distribution of chemotherapeutic agents *in vitro*. *Biochem Pharmacol.* 2003; 66(7):1207–1218. [PubMed: 14505800]
24. Raghunand N, Gillies RJ. pH and chemotherapy. *Novartis Found Symp.* 2001; 240:199–211. discussion 265–198. [PubMed: 11727930]
25. Raghunand N, Martinez-Zaguilan R, Wright SH, Gillies RJ. pH and drug resistance. II. Turnover of acidic vesicles and resistance to weakly basic chemotherapeutic drugs. *Biochem Pharmacol.* 1999; 57(9):1047–1058. [PubMed: 10796075]
26. Faber MD, Kupin WL, Heilig CW, Narins RG. Common fluid–electrolyte and acid–base problems in the intensive care unit: selected issues. *Semin Nephrol.* 1994; 14(1):8–22. [PubMed: 8140344]
27. Stacpoole PW. Lactic acidosis: the case against bicarbonate therapy. *Ann Intern Med.* 1986; 105(2):276–279. [PubMed: 3014943]
28. Smalley RV, Lefante J, Bartolucci A, Carpenter J, Vogel C, Krauss S. A comparison of cyclophosphamide, adriamycin, and 5-fluorouracil (CAF) and cyclophosphamide, methotrexate, 5-fluorouracil, vincristine, and prednisone (CMFVP) in patients with advanced breast cancer. *Breast Cancer Res Treat.* 1983; 3(2):209–220. [PubMed: 6688538]
29. Burghouts JT. Mitoxantrone, methotrexate and chlorambucil in metastatic breast cancer, a combination with relatively low subjective toxicity. *Netherlands J Med.* 1990; 36(1/2):43–45.
30. Taylor CW, Dalton WS, Mosley K, Dorr RT, Salmon SE. Combination chemotherapy with cyclophosphamide, vincristine, adriamycin, and dexamethasone (CVAD) plus oral quinine and verapamil in patients with advanced breast cancer. *Breast Cancer Res Treat.* 1997; 42(1):7–14. [PubMed: 9116320]
31. Phillips RM, Ward TH. Influence of extracellular pH on the cytotoxicity and DNA damage of a series of indolequinone compounds. *Anticancer Res.* 2001; 21(3B):1795–1801. [PubMed: 11497261]
32. Degani H, Gusic V, Weinstein D, Fields S, Strano S. Mapping pathophysiological features of breast tumors by MRI at high spatial resolution. *Nat Med.* 1997; 3(7):780–782. [PubMed: 9212107]
33. Eberhard A, Kahlert S, Goede V, Hemmerlein B, Plate KH, Augustin HG. Heterogeneity of angiogenesis and blood vessel maturation in human tumors: implications for antiangiogenic tumor therapies. *Cancer Res.* 2000; 60(5):1388–1393. [PubMed: 10728704]
34. Bhujwala ZM, Artemov D, Aboagye E, Ackerstaff E, Gillies RJ, Natarajan K, Solaiyappan M. The physiological environment in cancer vascularization, invasion and metastasis. *Novartis Found Symp.* 2001; 240:23–38. discussion 38–45, 152–153. [PubMed: 11727932]
35. Zhao J, Salmon H, Sarntinoranont M. Effect of heterogeneous vasculature on interstitial transport within a solid tumor. *Microvascular Res.* 2007; 73(3):224–236.
36. Garcia-Martin ML, Martinez GV, Raghunand N, Sherry AD, Zhang S, Gillies RJ. High resolution pH_e imaging of rat glioma using pH-dependent relaxivity. *Magn Reson Med.* 2006; 55(2):309–315. [PubMed: 16402385]
37. Kalman FK, Baranyai Z, Toth I, Banyai I, Kiraly R, Brucher E, Aime S, Sun X, Sherry AD, Kovacs Z. Synthesis, potentiometric, kinetic, and NMR Studies of 1,4,7,10-tetraazacyclododecane-1,7-bis(acetic acid)-4,10-bis(methylenephosphonic acid) (DO2A2P) and its complexes with Ca(II) , Cu(II) , Zn(II) and lanthanide(III) ions. *Inorg Chem.* 2008; 47(9):3851–3862. [PubMed: 18380456]
38. Kalman FK, Woods M, Caravan P, Jurek P, Spiller M, Tircso G, Kiraly R, Brucher E, Sherry AD. Potentiometric and relaxometric properties of a gadolinium-based MRI contrast agent for sensing tissue pH. *Inorg Chem.* 2007; 46(13):5260–5270. [PubMed: 17539632]
39. Martinez GV, Zhang X, Garcia-Martin ML, Morse DL, Woods M, Sherry AD, Gillies RJ. Imaging the extracellular pH of tumors by MRI after injection of a single cocktail of T_1 and T_2 contrast agents. *NMR Biomed.* 2011; 24(10):1380–1391. [PubMed: 21604311]

40. Frullano L, Catana C, Benner T, Sherry AD, Caravan P. Bimodal MR-PET agent for quantitative pH imaging. *Angew Chem Int Ed Engl.* 2010; 49(13):2382–2384. [PubMed: 20191650]
41. Gianolio E, Napolitano R, Fedeli F, Arena F, Aime S. Poly-beta-cyclo-dextrin based platform for pH mapping via a ratiometric ¹⁹F/¹H MRI method. *Chem Commun.* 2009; 40:6044–6046.
42. Liu G, Li Y, Sheth VR, Pagel MD. Imaging in vivo extracellular pH with a single paramagnetic chemical exchange saturation transfer magnetic resonance imaging contrast agent. *Mol Imaging.* 2012; 11(1):47–57. [PubMed: 22418027]
43. Sheth VR, Li Y, Chen LQ, Howison CM, Flask CA, Pagel MD. Measuring in vivo tumor pHe with CEST-FISP MRI. *Magn Reson Med.* 2012; 67(3):760–768. [PubMed: 22028287]
44. Aime S, Fedeli F, Sanino A, Terreno E. A R2/R1 ratiometric procedure for a concentration-independent, pH-responsive, Gd(III)-based MRI agent. *J Am Chem Soc.* 2006; 128(35):11326–11327. [PubMed: 16939235]
45. Ali MM, Woods M, Caravan P, Opina AC, Spiller M, Fettinger JC, Sherry AD. Synthesis and relaxometric studies of a dendrimer-based pH-responsive MRI contrast agent. *Chemistry.* 2008; 14(24):7250–7258. [PubMed: 18601236]
46. Caravan P, Farrar CT, Frullano L, Uppal R. Influence of molecular parameters and increasing magnetic field strength on relaxivity of gadolinium- and manganese-based T₁ contrast agents. *Contrast Media Mol Imaging.* 2009; 4(2):89–100. [PubMed: 19177472]
47. Hashim AI, Zhang X, Wojtkowiak JW, Martinez GV, Gillies RJ. Imaging pH and metastasis. *NMR Biomed.* 2011; 24(6):582–591. [PubMed: 21387439]
48. Raghunand N, Howison C, Sherry AD, Zhang S, Gillies RJ. Renal and systemic pH imaging by contrast-enhanced MRI. *Magn Reson Med.* 2003; 49(2):249–257. [PubMed: 12541244]
49. Rad AM, Arbab AS, Iskander AS, Jiang Q, Soltanian-Zadeh H. Quantification of superparamagnetic iron oxide (SPIO)-labeled cells using MRI. *J Magn Reson Imaging.* 2007; 26(2):366–374. [PubMed: 17623892]
50. Ali MM, Janic B, Babajani-Feremi A, Varma NR, Iskander AS, Anagli J, Arbab AS. Changes in vascular permeability and expression of different angiogenic factors following anti-angiogenic treatment in rat glioma. *PLoS One.* 2010; 5(1):e8727. [PubMed: 20090952]

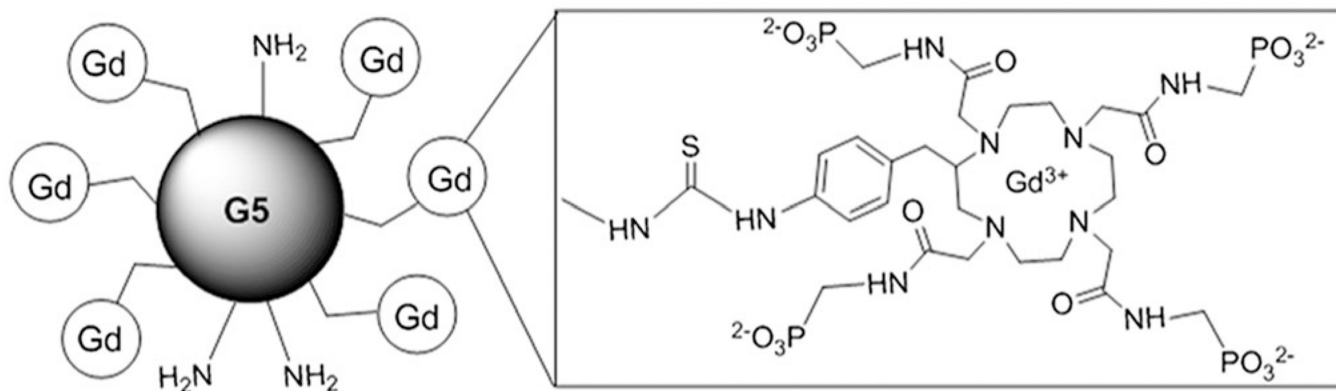


Figure 1. Schematic view of Gd³⁺ chelated with 1,4,7,10-tetraazacyclododecane-1,4,7,10-tetraaminophosphonate (DOTA-4AmP⁸⁻) in a G5PAMAM dendrimer.

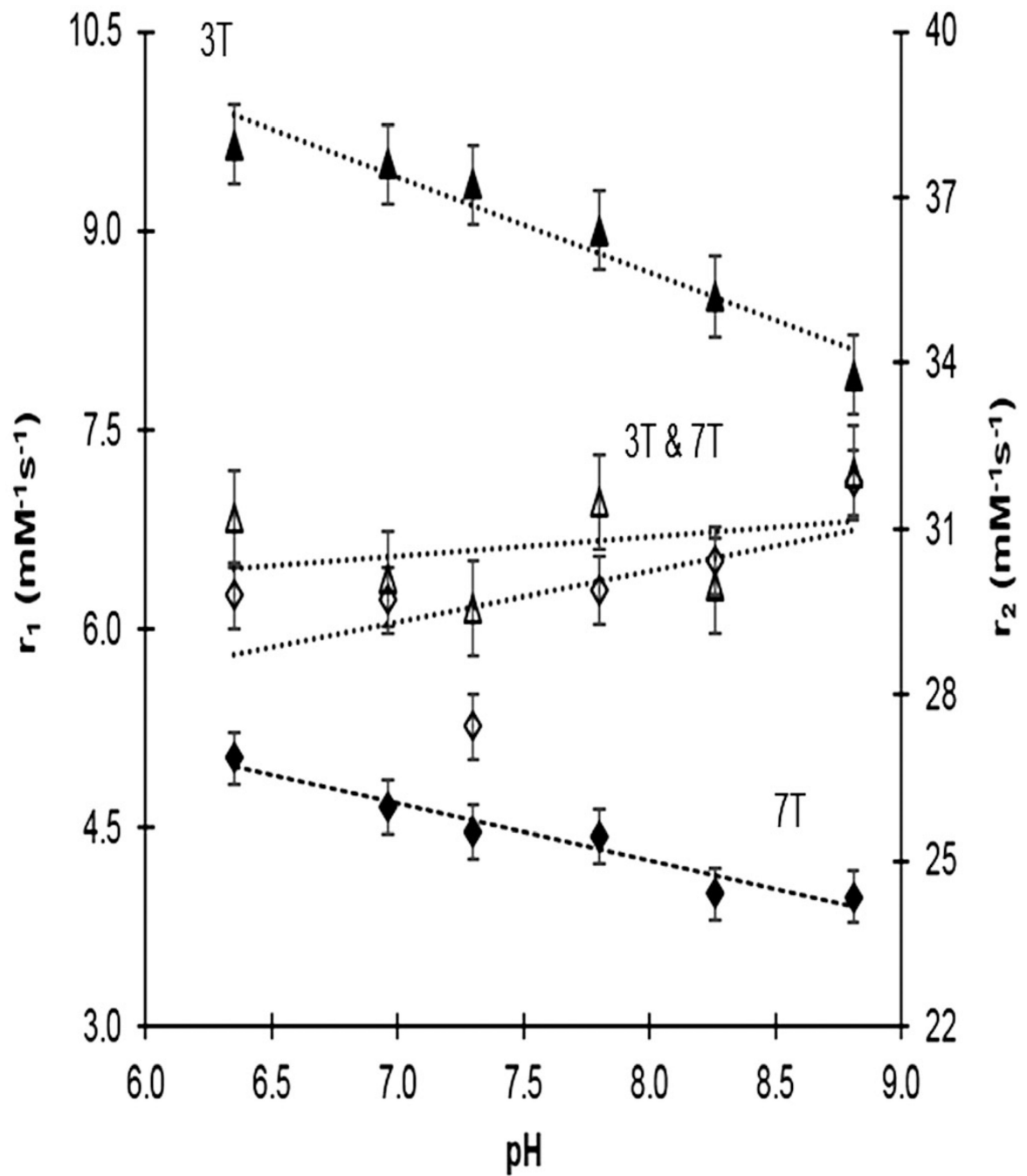


Figure 2. Longitudinal and transverse relaxivities (r_1 and r_2 , $\text{mM}^{-1}\text{s}^{-1}$) as a function of pH (6.35–8.84) in liquid phantoms measured at 3 T (triangles) and 7 T (diamonds), with linear regression fits to the data. Transverse relaxivity does not vary significantly with pH, or with field strength. The slopes of the longitudinal relaxivities do not differ between the field strengths.

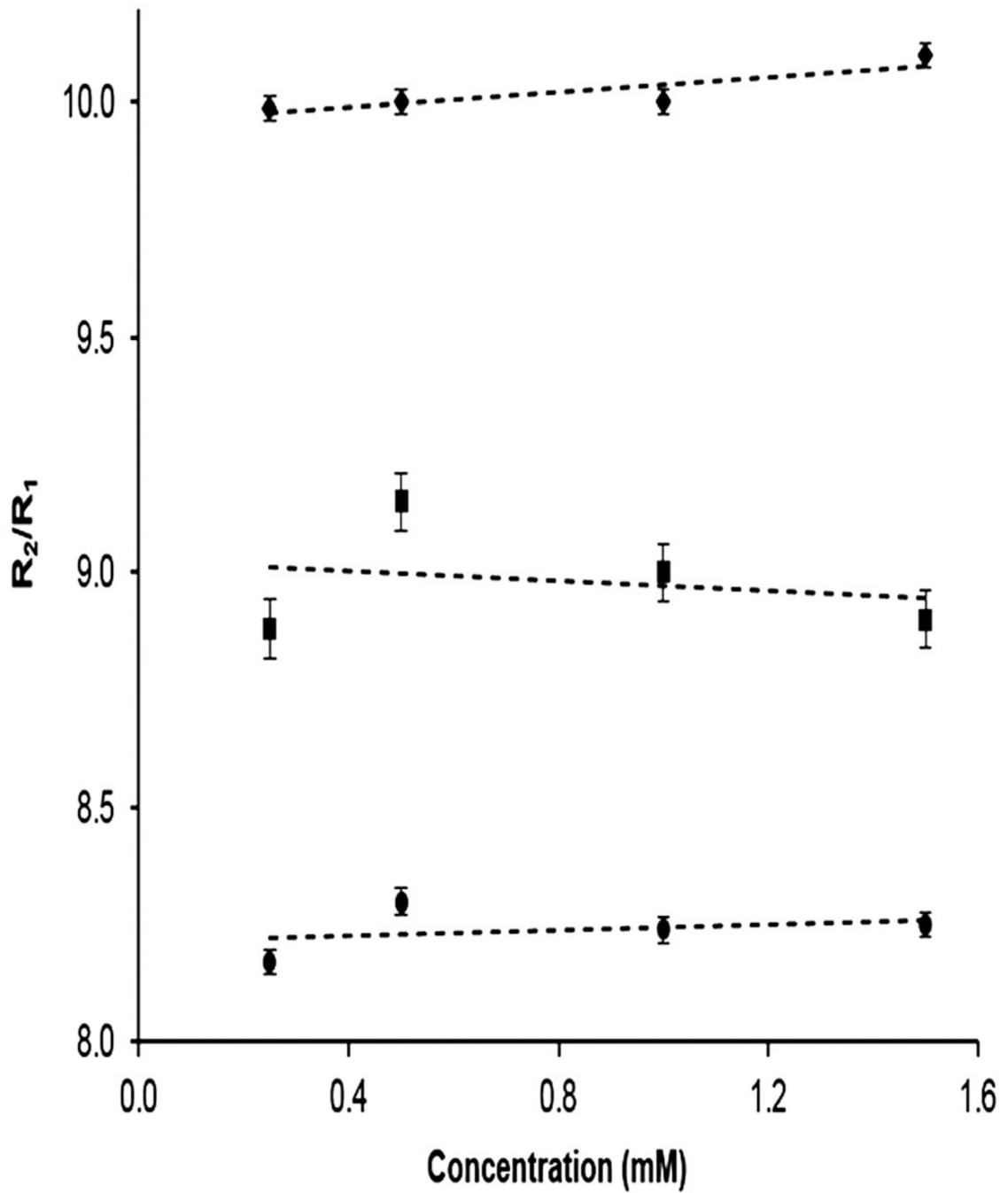


Figure 3.

The calculated ratio of R_2/R_1 for $(\text{Gd-DOTA-4AmP})_{44}\text{-G5}$ at four different concentrations and three different pH values at 7 T: top line, pH = 8.84, middle line, pH = 7.40, bottom line, pH = 6.96. The ratio R_2/R_1 does not vary significantly with concentration of contrast agent at the lower pH values, but there is a small and significant variation at the higher pH, which lies outside the range of values usually encountered in tumor tissues.

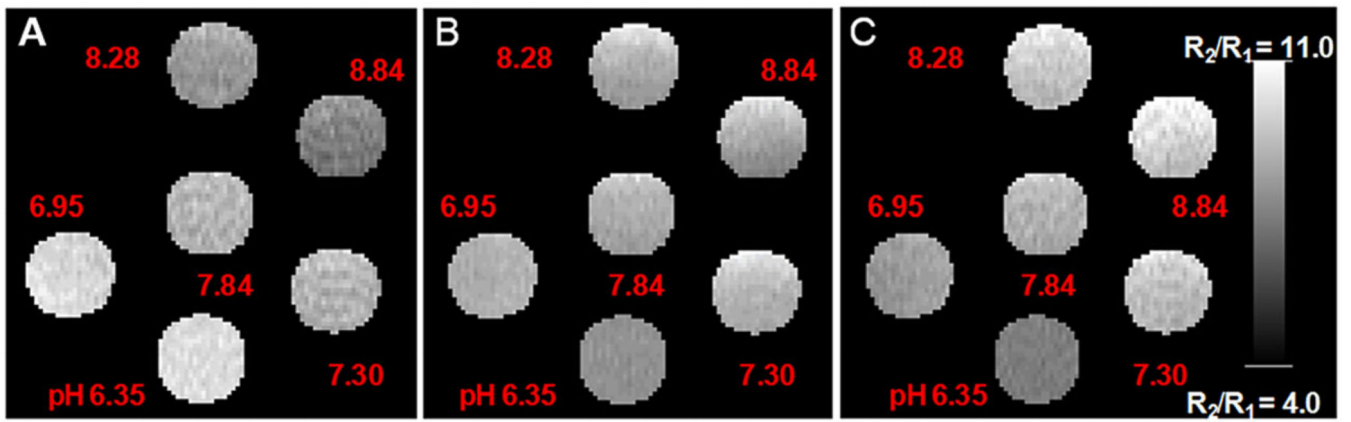


Figure 4. R_1 (A) and R_2 (B) maps generated from T_1 and T_2 -weighted images of phantoms containing 0.16 mM Gd_{44} -G5 at six different pH values. Average R_1 and R_2 values were calculated from hand-drawn ROIs. R_2/R_1 ratio maps at six different pH values were also generated (C).

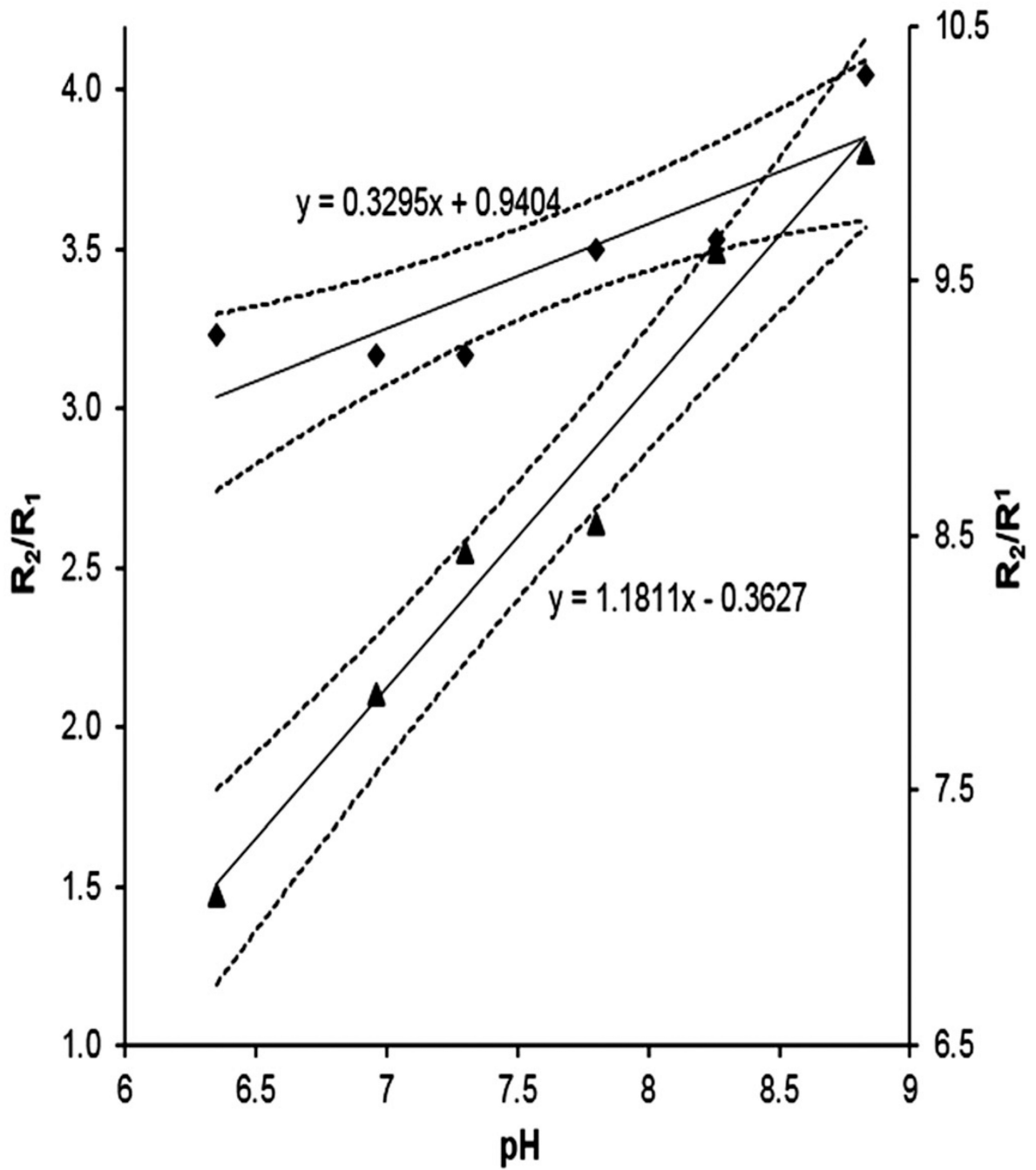


Figure 5.

R_2/R_1 versus pH plots. Left-hand ordinate, 3 T values; right-hand ordinate, 7 T values. The pH dependence of the relaxation rate ratio is shown with regression lines. Upper line (diamonds), 3 T data; bottom line (triangles), 7 T data. The 95% confidence intervals are plotted for both linear regressions.